In Vivo Dynamics and Differential Microtubule-Binding Activities of MAP65 Proteins[1]

Daniël Van Damme, Kris Van Poucke, Emmanuel Boutant, Christophe Ritzenthaler, Dirk Inzé*, and Danny Geelen

Department of Plant Systems Biology, Flanders Interuniversity Institute for Biotechnology, Ghent University, B–9052 Ghent, Belgium (D.V.D., K.V.P., D.I., D.G.); and Institut de Biologie Moleculaire des Plantes, F–67084 Strasbourg cedex, France (E.B., C.R.)

Plant cells produce different microtubule arrays that are essential for cell division and morphogenesis without equivalent in other eukaryotes. Microtubule-associated proteins influence the behavior of microtubules that is presumed to culminate into transitions from one array to another. We analyzed the microtubule-binding properties of three Arabidopsis (*Arabidopsis thaliana*) members, AtMAP65-1, AtMAP65-4, and AtMAP65-5, in live cells using laser scanning confocal microscopy. Depending on the overall organization of the cortical array, AtMAP65-1-GFP (green fluorescent protein) and AtMAP65-5-GFP associated with a subset of microtubules. In cells containing both coaligned and oblique microtubules, AtMAP65-1-GFP and AtMAP65-5-GFP tended to be associated with the coaligned microtubules. Cortical microtubules labeled with AtMAP65-1-GFP and AtMAP65-5-GFP appeared as thick bundles and showed more resistance to microtubule-destabilizing drugs. The polymerization rates of AtMAP65-1-GFP and AtMAP65-5-GFP microtubules were similar to those of tubulin-GFP marked microtubules but were different from AtEB1a-GFP, a microtubule plus-end-binding EB1-like protein that stimulated polymerization. By contrast, depolymerization rates of AtMAP65-1-GFP- and AtMAP65-5-GFP-labeled microtubules were reduced. AtMAP65-1-GFP associated with polymerizing microtubules within a bundle, and with fixed microtubule termini, suggesting that AtMAP65-1's function is to bundle and stabilize adjacent microtubules of the cortex. Polymerization within a bundle took place in either direction so that bundling occurred between parallel or antiparallel aligned microtubules. AtMAP65-4-GFP did not label cortical microtubules or the preprophase band, despite continuous expression driven by the 35S promoter, and its subcellular localization was restricted to microtubules that rearranged to form a spindle and the polar sides of the spindle proper. The expression of AtMAP65-4 peaked at mitosis, in agreement with a function related to spindle formation, whereas AtMAP65-1 and AtMAP65-5 were expressed throughout the cell cycle.

Microtubules are polar filamentous structures with a highly dynamic plus end and a more stable minus end. The plus end shows alternating phases of growth (polymerization) and rapid shortening (depolymerization), a phenomenon that is also known as dynamic instability. The dynamic instability of microtubules depends on two couples of mutually excluding parameters: the growth and shrinkage rate, and the frequencies at which a microtubule undergoes transitions between polymerization (growth phase) and depolymerization (shrinkage). The transition from a growing phase to shrinkage is termed catastrophy and from shrinkage phase to a growing phase termed rescue. The minus end is associated with microtubule organizing centers that nucleate microtubules. Microtubules are arranged into different arrays implicated in cell division and differentiation and hence are subject to various reorganizations. Plants have three unique microtubule arrays: the cortical array that forms a cage at the cell periphery in close association with the plasma membrane, the preprophase band surrounding the nucleus in cells entering a mitotic phase, and the phragmoplast consisting of two stacks of microtubules arranged in opposing orientation in between the separated daughter nuclei during cytokinesis (Goddard et al., 1994).

The cortical array of microtubules consists of parallel-arranged bundles rather than radial orientated microtubules. Cross-bridges between these microtubules and the plasma membrane ensure that the cortical array is shaped as a sheet instead of three-dimensional bundles (Cyr and Palevitz, 1995). Curiously, microtubules in the cortical array and the preprophase band are more dynamic than cytoplasmic microtubules in animal cells (Hush et al., 1994; Moore et al., 1997; Dhonukshe and Gadella, 2003). The peripheral microtubules in plant cells do not nucleate from microtubule organizing centers associated with a centrosome-like structure, but rather from multiple sites that are distributed throughout the cortex (Wasteneys, 2002). The minus end undergoes slow depolymerization, suggesting that microtubules are released from their nucleation centers unlike their animal counterparts (Shaw et al., 2003). The release of cortical microtubules from their nucleation centers

[1] This work was supported by the Fund for Scientific Research-Flanders (predoctoral and postdoctoral fellowships to D.V.D. and D.G., respectively).

* Corresponding author; e-mail dirk.inze@psb.ugent.be; fax 32–9–3313809.

Article, publication date, and citation information can be found at www.plantphysiol.org/cgi/doi/10.1104/pp.104.051623.

allows them to translocate along the cortex, but to achieve a specific coaligned organization of bundles, postnucleation events are necessary to transform the individual microtubules into the characteristic coaligned groups that make up the cortical array (Hardham and Gunning, 1978; Lloyd and Chan, 2004).

The contiguous attachment of linker proteins along adjacent microtubules may contribute to coaligned arrangement in the cortex. Cross-bridges have repetitively been reported to occur in electron microscopic observations of the cortical array (Cyr and Palevitz, 1995). Many biochemically purified microtubule-binding proteins have bundling activity in vitro and are potential candidates for accomplishing the cross-bridges (Vantard et al., 1993). For example, MOR1 is a 200-kD protein isolated from tobacco (*Nicotiana tabacum*) suspension cells that forms 10-nm cross-bridges in vitro between microtubules (Yasuhara et al., 2002). Recently, a new class of microtubule-associated proteins has been identified that binds the cortical array (Smertenko et al., 2000). These proteins have a molecular mass of about 65 kD and were therefore designated MAP65 (Chang-Jie and Sonobe, 1993). MAP65 proteins and their mammalian (PRC1) and yeast (ASE1) counterparts form filamentous cross-bridges that maintain a 25- to 30-nm distance between microtubules (Chan et al., 1999; Mollinari et al., 2002; Schuyler et al., 2003). The bundling of microtubules depends on a C-terminal domain that is also responsible for dimerization, suggesting that two molecules are needed for spanning a 25- to 30-nm distance (Smertenko et al., 2004). However, not all MAP65 proteins show bundling activity in vitro, like, for example, the tobacco NtMAP65-1a, although this protein was shown to dimerize with the Arabidopsis (*Arabidopsis thaliana*) AtMAP65-1 that does form cross-bridges (Smertenko et al., 2000, 2004). NtMAP65-1b bundles microtubules and protects them from cold-induced depolymerization but not from katanin-induced destabilization (Wicker-Planquart et al., 2004).

Arabidopsis has nine MAP65 proteins with predicted molecular masses from 54 to 80 kD (Hussey et al., 2002). AtMAP65-3 localizes at the spindle midzone and the phragmoplast midline, similar to NtMAP65-1, with the exception that NtMAP65-1 also associates with the cortical array (Smertenko et al., 2000; Müller et al., 2004). PLEIADE, identified as AtMAP65-3, is involved in cytokinesis and leads to the formation of multinucleated cells and incomplete cell walls when mutated (Müller et al., 2004). Previously, we have cloned seven Arabidopsis MAP65 genes and localized the green fluorescent protein (GFP)-tagged proteins in tobacco BY-2 cells (Van Damme et al., 2004). AtMAP1, 3, 5, and 8 labeled the cortical microtubule array. Here, we show that AtMAP65-1-GFP and AtMAP65-5-GFP associate with a subset of the cortical array. The AtMAP65-4-GFP protein does not label the cortical array and the preprophase band (PPB), but strongly associates with the perinuclear microtubules and the spindle in dividing cells. Fluorescence intensity measurement of microtubule tracks provides evidence that the in vivo microtubule-binding activity of MAP65 proteins depends on microtubule organization, microtubule number, and posttranslational regulation of the protein.

RESULTS

GFP-Tagged MAP65 Microtubule-Binding Proteins Label a Subset of the Cortical Array

Previously, we have localized members of the MAP65 protein family by expression of GFP-fusion constructs in BY-2 cells (Van Damme et al., 2004). The GFP-fusion products resulted in the differential labeling of cytoskeletal structures, suggesting that members of the MAP65 family have distinct microtubule-binding properties. To investigate the population of microtubules labeled by the GFP-fusion products, we imaged the GFP signal together with immunostained microtubules of BY-2 cells that produced either GFP-tagged tubulin (TUA6-GFP) or the AtMAP65-5-GFP fusion protein. Dual fluorescence imaging of microtubules decorated with anti-α-tubulin (red) and GFP-labeled microtubules (green) revealed that AtMAP65-5-GFP was associated with a subset of the cortical microtubules (Fig. 1A). The AtMAP65-5-GFP protein was predominantly associated with coaligned microtubules that were usually thicker than other microtubules crossing the cell in different directions. Transverse and obliquely oriented microtubules were labeled with TUA6-GFP as well as with the anti-α-tubulin antibody (Fig. 1B). Upon treatment of BY-2 cells carrying the MAP65-5-GFP construct with the severing drug oryzalin, microtubules were still clearly detected (Fig. 1C). Control cells that were treated likewise lost their TUA6-GFP-labeled microtubules almost completely (Fig. 1D). Thus, microtubules labeled with MAP65-5-GFP seemed more resistant to the severing drug oryzalin than nonlabeled microtubules. Next, we analyzed the sensitivity of microtubules to oryzalin in life cells by time-lapse microscopy. A short treatment of 90 min removed almost all microtubules in TUA6-GFP BY-2 cells (Fig. 1E). The same treatment applied to cells producing AtMAP65-5-GFP resulted in the incomplete depolymerization of the labeled microtubules (Fig. 1F). The remnant microtubules were more intensively labeled and appeared as thick bundles.

AtMAP65-1-GFP and AtMAP65-5-GFP Associate Preferentially with Coaligned Microtubules

To determine the localization and to investigate the behavior of the MAP65 proteins in life cells, we coexpressed the GFP chimers together with monomeric red fluorescent protein (RFP; Campbell et al., 2002)-tagged tubulin (TUA2 and TUA6) or with RFP-tagged microtubule-binding domain (MBD) of MAP4. Introduction of TUA2-RFP, TUA6-RFP, and RFP-MBD in BY-2 allowed the visualization of homogeneously

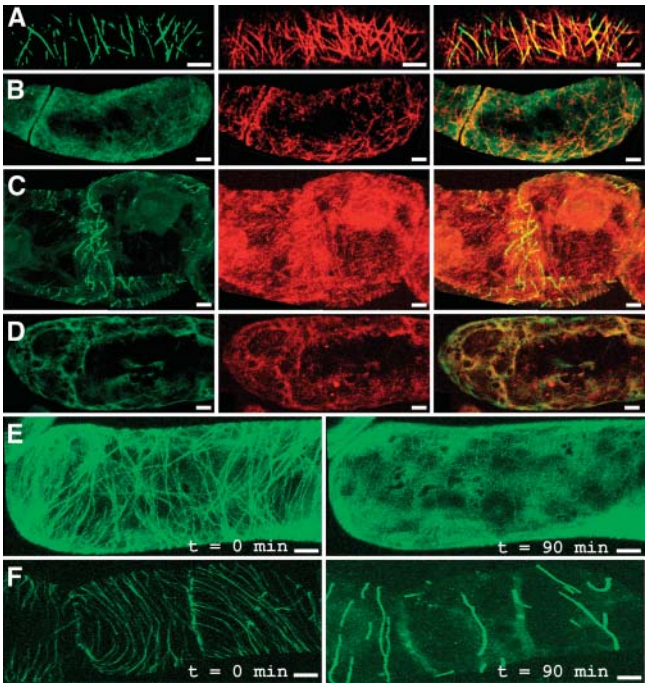

Figure 1. AtMAP65-5-GFP labels a subset of cortical microtubules with increased resistance to the microtubule drug oryzalin. TUA6-GFP and AtMAP65-5-GFP expressing BY-2 cells were immunostained with anti-α-tubulin antibody and observed under a laser confocal microscope. Green signal is GFP fluorescence and red signal is anti-tubulin antibody. The yellow signal is the overlap of green and red. A, AtMAP65-5-GFP. B, TUA6-GFP. C, AtMAP65-5-GFP treated for 90 min with 10 μM oryzalin. D, TUA6-GFP treated for 90 min with 10 μM oryzalin. E, TUA6-GFP fluorescence of live BY-2 cell observed before and after oryzalin treatment. F, AtMAP65-5-GFP fluorescence of live BY-2 cell observed before and after oryzalin treatment. Scale bars = 5 μm.

fluorescent cortical microtubules in the cell periphery (data not shown). The TUA2 fusion protein tended to give more specific microtubule labeling displaying lower background fluorescence in the cytoplasm than did TUA6-RFP. BY-2 suspension cultures producing RFP-MBD and TUA2-RFP were transformed with the AtMAP65-1-GFP, AtMAP65-4-GFP, and AtMAP65-5-GFP constructs. AtMAP65-1-GFP and AtMAP65-5-GFP strongly labeled the transversely organized cortical microtubules (Fig. 2). The microtubule bundles appeared to be thicker than those observed in cells producing TUA2-RFP or RFP-MBD alone (data not shown). BY-2 cells producing AtMAP65-4-GFP did not label cortical microtubules, although microtubules at the nuclear periphery were labeled (see below). Recording of the green and red fluorescence channels separately showed that AtMAP65-1-GFP and AtMAP65-5-GFP were bound to a subset of cortical microtubules (Fig. 2). The abundance of microtubules not labeled with MAP65-1-GFP and MAP65-5-GFP varied from cell to cell and was most obvious in cells with oblique-arranged microtubules (Fig. 2). In cells with predominantly transverse-arranged microtubules, the overlap of both AtMAP65-1-GFP and AtMAP65-5-GFP with the TUA2-RFP fluorescence was the highest (Fig. 2). In these cells we also noticed that the majority of non-MAP65-labeled microtubules were oblique. To have an impression on the suspected preference for coaligned microtubules, we counted the number of clearly oblique versus coaligned microtubules (220 microtubules in 4 different cells). Approximately 30% of the TUA2-RFP-labeled microtubules were oblique, whereas this was only 5% for the AtMAP65-1-GFP-labeled microtubules. The population of the TUA2-RFP-labeled microtubules that was not detected in the green fluorescence channel remained dark even after increasing the detector sensitivity to its maximum, indicating that AtMAP65-1-GFP did not label these microtubules (data not shown). Fully expanded and elongated cells had predominantly transverse microtubules and showed strong colocalization of MAP65-1-GFP and TUA2-RFP, whereas rounded cells often had oblique microtubules with much less overlap. Thus, microtubule

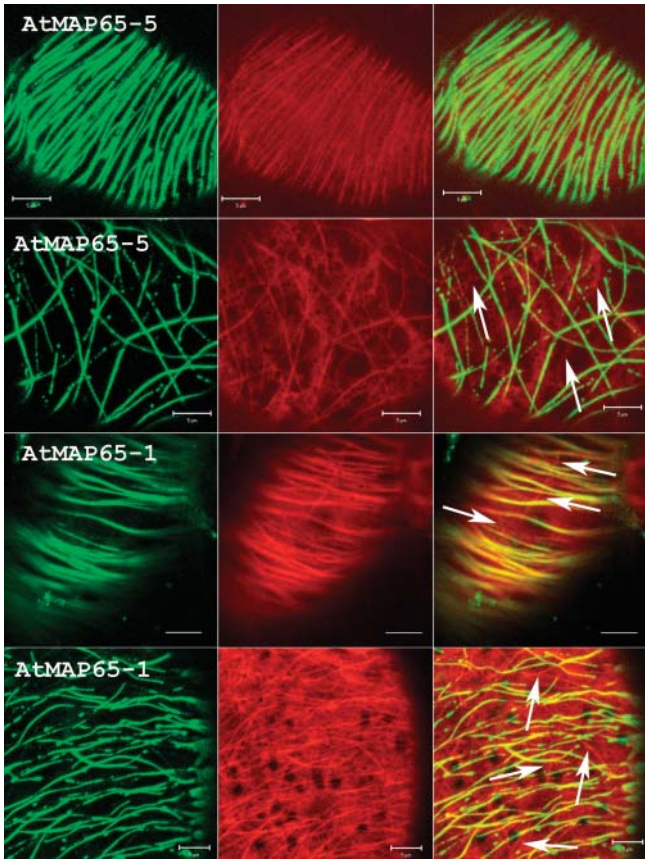

Figure 2. Preferential association of AtMAP65-1-GFP and AtMAP65-5-GFP with transverse microtubules. Confocal projections of the cortical array labeled with TUA2-RFP (red signal) together with AtMAP65-5-GFP (two rows at top) or AtMAP65-1-GFP (two rows at bottom). The third column presents the overlay of red and green fluorescence. A complete overlap occurs in cells with predominantly transversely organized microtubules, whereas cells with oblique microtubules are only partially stained with the AtMAP65-GFP fusion proteins (white arrows). Scale bars = 5 μm.

association of AtMAP65-1 and AtMAP65-5 shows preference for coaligned microtubules.

AtMAP65-1 Confers Resistance to the Microtubule Drug Propyzamide

Some of the AtMAP65-5-GFP microtubules appeared to be resistant to degradation by the microtubule drug oryzalin (Fig. 1). To analyze the drug sensitivity of microtubules labeled with AtMAP65-1-GFP in live cells, BY-2 cultures that coexpressed AtMAP65-1-GFP and TUA2-RFP were treated with amiprophos-methyl and propyzamide. Amiprophos-methyl is a phosphoroamidate with an action similar to that of the closely related oryzalin, a dinitroaniline (Morejohn, 1991) that binds to plant α-tubulin and affects protofilament interactions (Anthony and Hussey, 1999). Propyzamide, on the other hand, is a benzamide that may have a more subtle effect on microtubule polymerization, as transversely organized microtubules are better protected against its action (Furutani et al., 2000). In the presence of amiprophos-methyl or propyzamide, cortical microtubules of control cells producing TUA2-GFP decayed within 30 min (Fig. 3). By contrast, some microtubules in cells producing AtMAP65-1-GFP remained despite the microtubule drugs. Degradation was apparent in amiprophos-methyl-treated cells, resulting in the accumulation of fluorescent dots (Fig. 3). Propyzamide caused a weaker effect, with most of the microtubules labeled with AtMAP65-1-GFP still intact after 2 h, although the fluorescence intensity was reduced (Fig. 3). Thus, expression of AtMAP65-1-GFP stabilizes and increases drug resistance of microtubules.

AtMAP65 Is Incorporated into Stable Microtubule Bundles

Upon viewing a number of video recordings of the cortical array from AtMAP65-1-GFP and AtMAP65-5-GFP cells, we noticed that the frequency at which newly formed microtubules coming into the scanned field was lower than that observed in TUA2-GFP and GFP-MBD cells. To have an impression on the dynamics of the cortical array, we measured the abundance of microtubule bundles accumulated in a time frame of 10 min by counting the number of fluorescent tracks that crossed a 20-μm bar placed perpendicular to the long axis of a fully expanded cell. In 26 recordings, an average of 19.4 (SD = 5.6) GFP-MBD-labeled microtubules crossed the 20-μm bar (Fig. 4A). The number of microtubules counted in MAP65-GFP-labeled cells was significantly lower: 16.1 (n = 16; SD = 3.9) in AtMAP65-1-GFP and 16.3 (n = 20; SD = 4.6) in cells

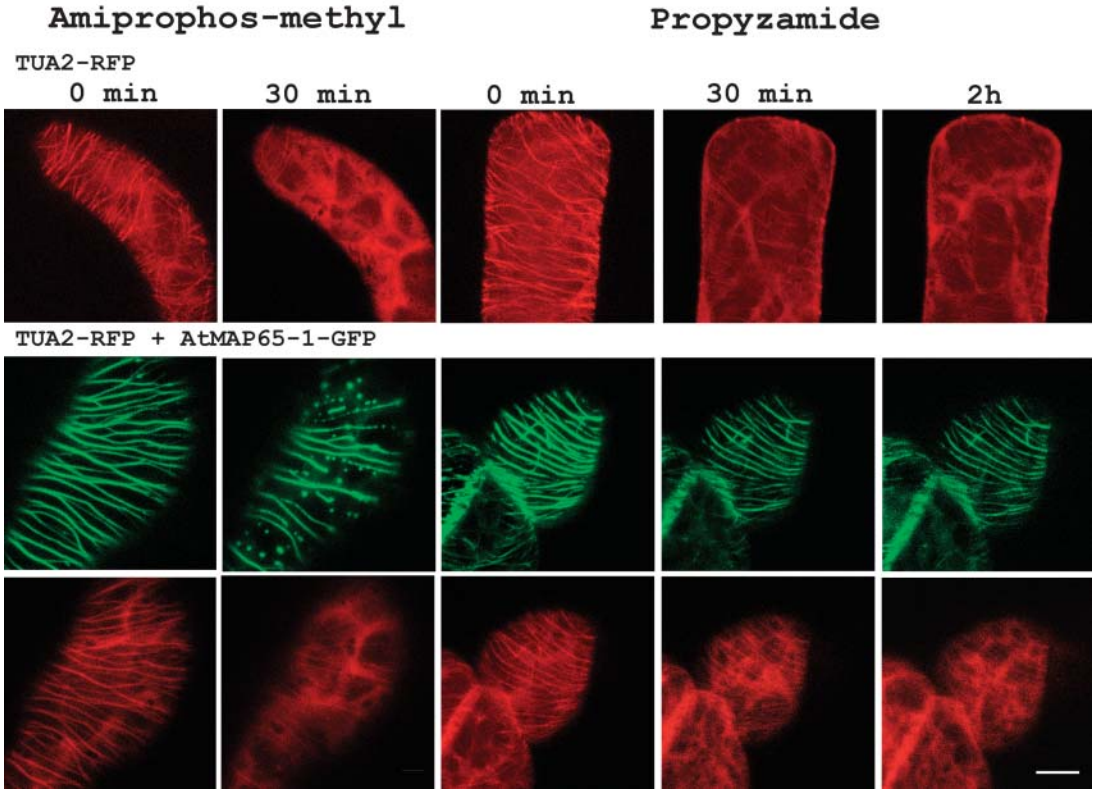

Figure 3. Resistance to microtubule polymerization drugs conferred by AtMAP65-1-GFP. Confocal projections of BY-2 cells expressing TUA2-RFP (red signal) or TUA2-RFP together with AtMAP65-1-GFP (green signal). Cells were treated with either amiprophos-methyl or propyzamide. Images were taken at 30 min or 2 h after adding the drugs. Bar = 10 μm.

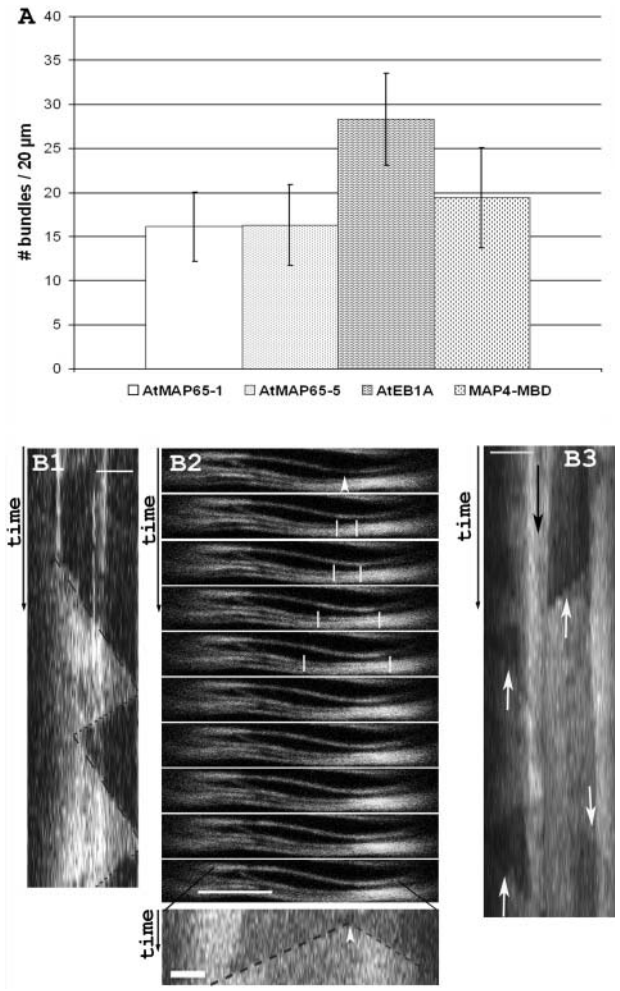

Figure 4. Dynamics of AtMAP65-1-GFP-labeled microtubule bundles. A, Graph showing the number of microtubule tracks that crossed a 20-μm bar in a 10-min time frame in the cortex of cells expressing AtMAP65-1-GFP, AtMAP65-5-GFP, AtEB1a-GFP, and GFP-MAP4-MBD. B1, Kymograph of a 10-min recording of a AtMAP65-1GFP fluorescent track showing consecutive depolymerization and polymerization events within a microtubule bundle. The dashed lines indicate polymerization and the dotted lines depolymerization. Bar = 5 μm. B2, Microtubules initiate and polymerize in opposite directions within a microtubule bundle. Consecutive images of 20-s interval show the polymerization of two microtubules. The arrowhead marks the point of initiation. The kymograph shows the fluorescence intensity changes over time of the trace marked by white vertical bars. Polymerization is from left to right and from right to the left (dashed lines). Image series, bar = 5 μm; kymograph, bar = 2 μm. B3, Kymograph of a AtMAP65-1-GFP track with complex fluorescence pattern. Microtubule dynamics were monitored over a 10-min time period. The black arrow points out a pausing microtubule; the white arrows indicate different microtubule polymerization and depolymerization events. Bar = 5 μm.

producing AtMAP65-5-GFP. An average of 28 microtubules (n = 19; SD = 5.2) crossed a 20-μm bar in cells producing AtEB1a-GFP, suggesting that expression of AtEB1a-GFP stimulated microtubule polymerization dynamics (Fig. 4A). A more detailed observation of the fluorescence tracks in the time-lapse recordings from AtMAP65-1-GFP and AtMAP65-5-GFP BY-2 cells revealed changes in GFP fluorescence in the labeled microtubule bundles, consistent with growth and shrinkage of microtubules alongside the bundle. We digitally linearized a number of fluorescence tracks and plotted these against time in separate kymographs (Fig. 4B). The kymograph shown in Figure 4B1 illustrates a fluorescent track with relatively simple polymerization and depolymerization dynamics of an individual microtubule that lies within an existing microtubule bundle. Polymerization and depolymerization occurred in the two directions within the same microtubule bundle (Fig. 4B2). The kymograph in Figure 4B2 (arrowhead) identifies a position on the microtubule that appears to be a nucleation site from which two microtubules polymerize in opposing directions. Many of the track histories were difficult to interpret because of a relatively high background fluorescence of the microtubule bundle and because each track carried the life history of multiple microtubules (Fig. 4B3). These data indicate high dynamicity of adjacent microtubules within a microtubule bundle. As there were relatively few new fluorescent tracks appearing in our recordings, it is possible that most AtMAP65-1-GFP and AtMAP65-5-GFP-labeled microtubules initiated at positions near or on the cortical microtubules. Microtubule initiation sites occur in association with existing microtubules but can also be independent from microtubules (Shaw et al., 2003). Microtubule nucleation independent from existing microtubules was not found in BY-2 cells producing MAP65-1-GFP and AtMAP65-5-GFP, probably because such sites do not involve polymerization of bundled microtubules.

MAP65-1-GFP Concentrates in Dot-Like Structures and Is Unequally Distributed along Microtubules

Microtubules labeled with MAP65-1-GFP often carried hot spots of fluorescence that appeared as dots along a weakly fluorescing track. Occasionally dots were also seen in cells producing AtMAP65-5-GFP, but these occurred less frequently. The abundance of the AtMAP65-1-GFP spots varied from cell to cell and they were mostly within or adjacent to microtubule bundles (Fig. 5A, arrowheads), although some were also apparently not connected to labeled microtubules (Fig. 5A, arrow). In 22 time-lapse recordings that we screened for fluorescent spots, none of them was mobile during the course of monitoring (usually 10 min; Fig. 5B), indicating that they were different from the rapidly moving microtubule plus ends or the slow-moving minus ends (Shaw et al., 2003). The absence from dynamic microtubule plus ends was further confirmed in transiently transfected tobacco epidermal cells carrying combinations of the MAP65-GFP and AtEB1a-RFP fusion constructs. The AtMAP65-1-GFP spots that were observed in this experimental setup were not labeled with AtEB1a-RFP (data not shown), and we did not observe microtubule initiation emanating from the spots, so they must be different

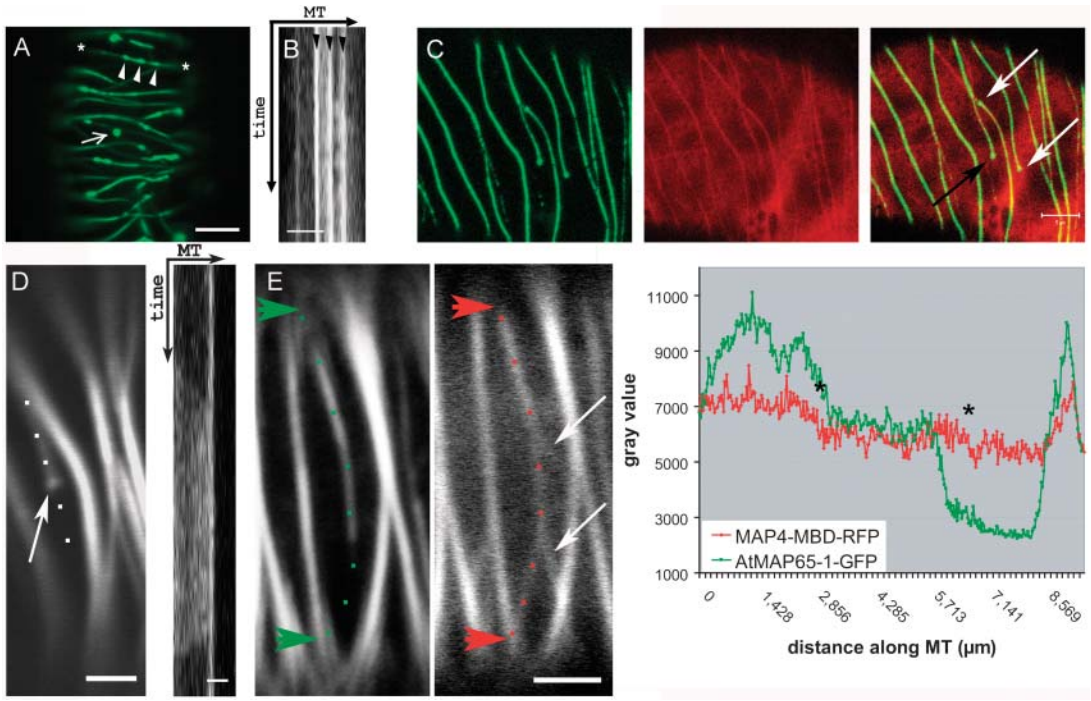

Figure 5. Differential distribution of AtMAP65-1-GFP along microtubule bundles. A, Collapsed time lapse of 50 images (490 s) of a subregion of the cortical array in a AtMAP65-1-GFP BY-2 cell. Hot spots of AtMAP65-1-GFP fluorescence are indicated with white arrowheads (bar = 5 μm). B, Kymograph of the microtubule bundle indicated in A between white asterisks. Black arrowheads indicate immobile fluorescent spots occurring on the selected microtubule. Bar = 5 μm. C, Collapsed Z-stack (3.47 μm) of double-labeled cortical microtubules in AtMAP65-1-GFP (green) and TUA2-RFP (red). The overlay image shows a spot at the end of a microtubule bundle indicated with a black arrow. The two white arrows indicate the apparent end of microtubule labeled with AtMAP65-1-GFP that is associated with an extending TUA2-RFP-labeled microtubule bundle. Bar = 5 μm. D, Collapsed time lapse (650 s) of a subregion of the cortical array in a AtMAP65-GFP BY-2 cell. The white arrow indicates a hot spot of fluorescence that coincides with the position where a polymerizing microtubule is stopped. The dotted line indicates the track used to generate the kymograph. A microtubule is shown to polymerize up to the immobile fluorescent spot and then subsequently it depolymerizes. Bars = 2 μm. E, Collapsed time lapse of 60 images (590 s) and the relative RFP-MBD (red) and AtMAP65-1-GFP (green) fluorescence of a microtubule bundle indicated by the dotted line between red and green arrowheads. Connecting microtubules are indicated with white arrows. The positions where the connecting microtubules join the bundle are indicated with black asterisks. Bar = 2.5 μm.

from the nucleation sites described before (Shaw et al., 2003). Some spots appeared to localize to the end of a microtubule (black arrow, Fig. 5C). The AtMAP65-1-GFP spots also marked microtubule ends that occurred within a bundle (white arrows, Fig. 5C). In several occasions we observed that microtubules polymerizing within a bundle paused at the position of a strongly fluorescent spot and subsequently started to depolymerize (Fig. 5D). Analysis of the fluorescence intensity plots of the microtubule tracks further revealed that AtMAP65-1-GFP label varied along with the red RFP-MBD label over a distance within the same microtubule bundle. Figure 5E illustrates the intensity in AtMAP65-1-GFP (green) and RFP-MBD (red) fluorescence within the same track, recorded over a time period of 10 min. The MAP65-1-GFP (green) and the RFP-MBD (red) signals showed two consecutive reductions in intensity, albeit it was more pronounced for AtMAP65-1-GFP (Fig. 5E). The shifts in fluorescence coincided with the positions where a microtubule joined the bundle as if it was dependent on the density or number of microtubules within the bundle (Fig. 5E, arrows). The increase in green signal from AtMAP65-1-GFP fluorescence corresponded to the relative amplitude of the red signal from RFP-MBD, indicating that they were interrelated. In fact, the trace with the weakest fluorescence signal might correspond to a single microtubule that on its own does not suffice for AtMAP65-1-GFP binding (Fig. 5E). The data suggest that AtMAP65-1-GFP associates with adjacent microtubules and concentrates at stable microtubule ends.

MAP65-Labeled Microtubules Display Reduced Depolymerization Dynamics

The increases and decreases in length of fluorescent tracks occurring in interphase cells over a time period of 10 min were taken as a measure for the rate of polymerization and depolymerization, respectively. Data were collected from microtubules labeled with GFP-MBD, AtEB1a-GFP, AtEB1b-GFP, AtMAP65-1-GFP, and AtMAP65-5-GFP in BY-2 cells that were

cultivated and observed under similar experimental conditions. The microtubule shown in Figure 4B1 displayed a polymerization speed of 4.16 μm min^{-1} and 3.86 μm min^{-1} in the first and the second events, respectively. The shrinkage rate of the same microtubule in Figure 4B1 was 6.98 μm min^{-1} and 7.32 μm min^{-1}. These latter values are about one-half of that measured for control markers, suggesting that AtMAP65-5-GFP-labeled microtubules had a reduced depolymerization speed. The catastrophe and rescue events of microtubules growing and shrinking along existing bundles were difficult to measure because of the high background fluorescence from neighboring fibers and because of the complexity of the variations in fluorescence intensity (see above). We therefore determined the dynamicity parameters more accurately from newly appearing microtubule tracks that were not visibly in contact to other microtubules. Polymerization and depolymerization speeds were determined from at least three individual tracks per cell. These values were averaged for $n = 13$ cells and used to calculate the average speeds (Table I). Figure 6 shows the frequency at which a given average speed was recorded per cell. From Table I, it can be inferred that GFP-MBD microtubules grow at an average speed of 3.9 μm min^{-1} and shrink at 18 μm min^{-1} (Table I). Application of ANOVA statistics and Sheffy analysis on the raw data set classified AtMAP65-1-GFP and AtMAP65-5-GFP polymerization rates together with the result from GFP-MBD. Depolymerization rate on the other hand was found to be significantly different (Table I; Fig. 6). Thus, the AtMAP65-1-GFP and AtMAP65-5-GFP depolymerization rate was reduced for microtubules that had newly appeared as well as for those embedded in preexisting bundles. AtEB1a-GFP-labeled microtubules polymerized at an average speed of 5.3 μm min^{-1}. This is significantly faster than tubulin-GFP-labeled microtubules (Table I; Hush et al., 1994; Dhonuhske and Gadella, 2003; Shaw et al., 2003). The stimulatory effect on polymerization was specific to AtEB1a, as AtEB1b did not display increased growth rates (Table I). Depolymerization rates and transition frequencies could not be analyzed for microtubules labeled with AtEB1a and AtEB1b because these proteins were removed from the microtubule plus end upon catastrophy. Catastrophy and rescue of microtubules labeled with AtMAP65-1-GFP and AtMAP65-5-GFP were calculated from the inverse of the mean time spent in shrinkage and the mean time in growth, respectively (Cassimeris et al., 1988; Table I). A significant reduction in rescue frequency was evident for microtubules labeled with AtMAP65-1-GFP and AtMAP65-5-GFP compared to GFP-MBD-labeled microtubules. Together, these data indicate that cortical microtubules show distinct dynamic behavior depending on whether they are labeled with GFP-MBD, AtMAP65, or AtEB1.

MAP65-4 Transcription Is Activated during Mitosis

The presence of a conserved destruction box in several of the MAP65 family members is indicative of the regulation of protein abundance throughout the course of the cell cycle. The tobacco cyclin B1 protein, for example, has been shown to carry a functional destruction box (RXXLXX(L/I)XN) that is essential for its degradation at the onset of anaphase by the 26S proteasome complex (Genschik et al., 1998; Criqui et al., 2000). We found a conserved D box (**R**SQL**G**EL**QN**) in the N terminus of the AtMAP65-4 sequence. In addition to posttranslational control, B-type cyclins are also regulated at the transcriptional level (Shaul et al., 1996; Ito et al., 1998). We therefore decided to analyze the RNA profiles of the AtMAP65 transcripts using publicly available Affymetrix (Santa Clara, CA) microarray data of synchronized Arabidopsis tissue culture cells (Menges et al., 2003). Figure 7 shows the expression profiles that were retrieved for AtMAP65-1, AtMAP65-4, AtMAP65-5, and CYCB1;4. AtMAP65-4 was coactivated with cycB1;4 at the onset of mitosis, 8 h after release from the aphidicolin block (Fig. 7). AtMAP65-1 showed a moderate increase in expression, peaking at mitosis. By contrast, AtMAP65-5 expression was reduced from S-phase through M-phase. It contains a conserved D-box sequence (**R**AD**L**QD**L**R**N**) at a similar position as AtMAP65-4. Expression of MAP65 is therefore most likely regulated at the transcriptional and posttranslational level.

MAP65-4-GFP Specifically Associates with the Spindle Microtubules

Cortical array microtubules are not decorated by MAP65-4-GFP despite continuous expression driven by the 35S promoter and production of the MAP65-4-GFP protein (data not shown). However,

Table I. *Microtubule instability parameters*

	Polymerization[a]		Depolymerization[a]		Catastrophy[b]	Rescue[b]
	Average	Variance	Average	Variance	Average	Average
GFP-MBD	3.93	0.46	18.05	4.38	0.023	0.051
AtMAP65-1-GFP	4.22	1.07	9.93	2.69	0.023	0.030
AtMAP65-5-GFP	3.45	0.72	8.90	3.16	0.031	0.024
AtEB1a-GFP	5.28	0.27	–[c]	–	–	–
AtEB1b-GFP	3.37	0.39	–	–	–	–

[a]Velocity expressed as μm s^{-1}. [b]Frequency expressed as s^{-1}. [c]–, Not determined.

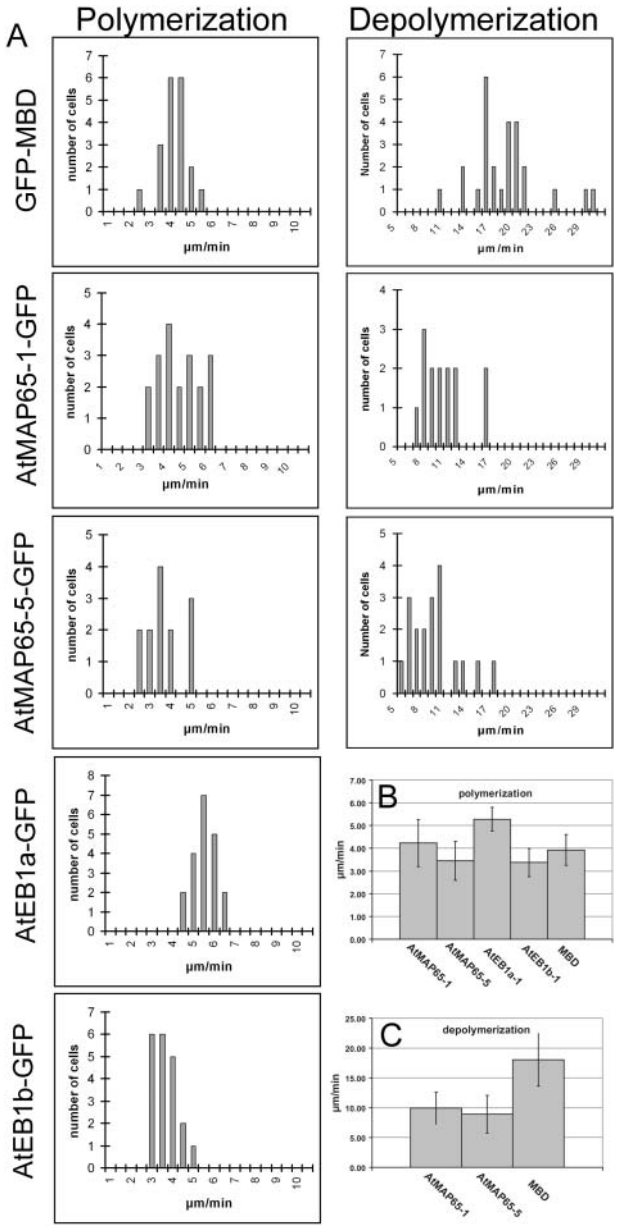

Figure 6. Microtubule polymerization and depolymerization dynamics. A, Histograms of microtubule growth rate (polymerization) and shrinkage rate (depolymerization) obtained from different BY-2 cells. Microtubules labeled with GFP-MBD, AtMAP65-1-GFP, AtMAP65-5-GFP, AtEB1a-GFP, and AtEB1b-GFP were measured. The *y* axis gives the frequency at which a certain average speed (*x* axis, in μm min^{-1}) per cell occurred. B and C, Histogram with the average polymerization and depolymerization speed, respectively, obtained for the different transgenic lines.

a distinct fluorescence pattern developed during early events of the preprophase (Fig. 8). At that time of the cell division program, the preprophase band is still present and appears as a narrow band at either side of the nucleus in optical confocal sections (Fig. 8, t = 0 min). The preprophase band contains microtubules labeled with TUA2-RFP and was slightly labeled with AtMAP65-4-GFP. Much stronger GFP fluorescence labeling occurred at the perinuclear array where nuclear microtubules start to assemble into a bipolar spindle structure. The AtMAP65-4-GFP protein was unevenly distributed at the periphery of the nucleus very early at the beginning of microtubule organization, when the nuclear envelope is intact and the remains of the degrading PPB are still visible (Fig. 8, t = 7). The two poles of the plant spindle are not focused into a single point like in yeast or metazoan cells but wider and more loosely arranged. AtMAP65-4-GFP was associated with the spindle microtubules and preferentially localized to the spindle poles. The concentration at the poles became more evident as the metaphase progressed into anaphase and chromosomes separated (Fig. 8, t = 46). AtMAP65-4-GFP was not associated with spindle microtubules that connect the two poles (Fig. 8, t = 42, 46). At the end of anaphase, AtMAP65-4-GFP dissociated from the spindle and either disappeared into the cytoplasm or was proteolytically removed. Thus, the primary function of AtMAP65-4 function is restricted to mitosis and more specifically to spindle formation.

DISCUSSION

The cortical array is a network of microtubules located underneath the plasma membrane that typically is arranged as transverse bundles in differentiated and elongated cells. This type of organization is susceptible to environmental changes and is broken down and restructured when the cell divides. Prior to the establishment of a coalignment of the peripheral microtubules, the arrangement seems temporary disorganized, indicating that the coalignment of microtubules

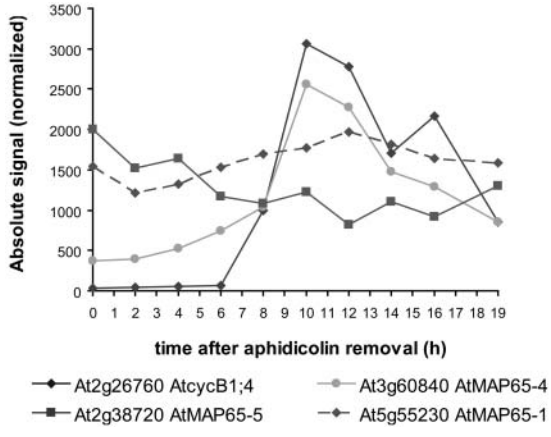

Figure 7. Transcript levels of AtMAP65 family members through the cell cycle. Arabidopsis cell suspension cultures were chemically synchronized in the presence of DNA polymerase inhibitor aphidicolin. Transcript levels of AtMAP65-1, AtMAP65-4, and AtMAP65-5 were quantified before and after release from the S-phase block with Affymetrix microarray chips, as described by Menges et al. (2003). The expression profile of AtcycB1;4 was included as a reference for mitosis-specific expression.

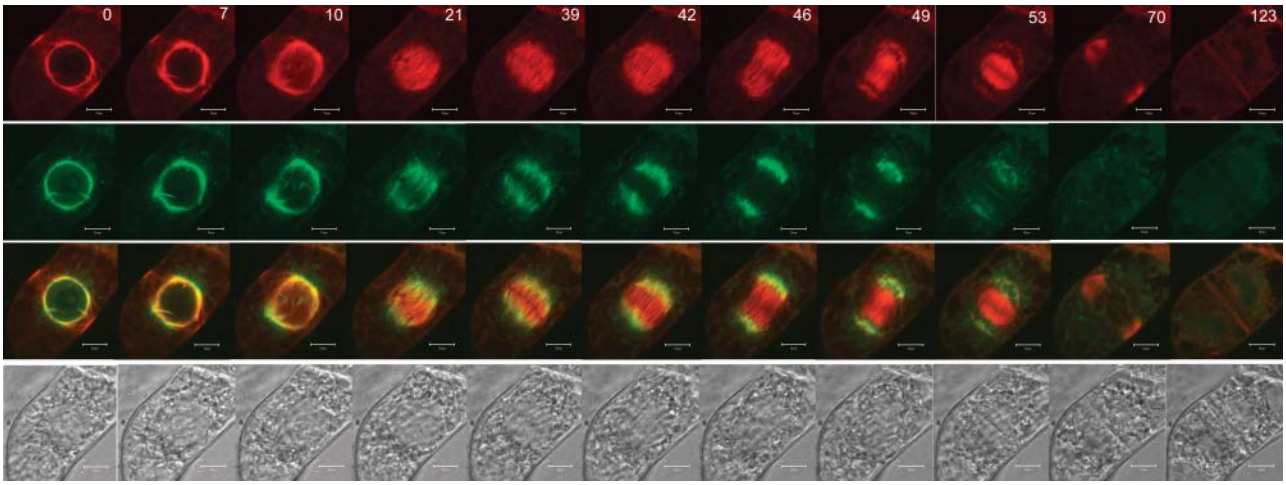

Figure 8. Specific binding of AtMAP65-4-GFP to spindle microtubules. Time-lapse recording of a BY-2 cell producing TUA2-RFP (red signal) and AtMAP65-4-GFP (green signal). Time points are indicated in the top right corner in minutes. The yellow signal in the overlay is colocalization. The row at the bottom shows differential interference contrast images. Bar = 10 μm.

is a self-organizing process. How this remodeling takes place is not understood, but microtubule motility and dynamics that are modulated by microtubule-associated proteins are important. Here, we provide evidence that the microtubule-binding proteins AtMAP65-1 and AtMAP65-5 associate with a subset of cortical microtubules. A third member of the MAP65 family that we analyzed, AtMAP65-4, is excluded from the cortical array and the PPB, and binds specifically to the perinuclear and spindle microtubules in mitotic cells. These observations indicate a differentiation in the microtubule-binding activity of MAP65 proteins. The microtubule-binding activity may be exclusive for certain microtubule arrays and selective for particular microtubules within an array.

MAP65 proteins were first discovered in tobacco BY-2 cell suspension protein extracts precipitated with taxol-stabilized microtubules (Chang-Jie and Sonobe, 1993). In the presence of MAP65 protein, the microtubules arranged adjacent to each other and were linked through cross-bridges as was viewed in electron micrographs (Chang-Jie and Sonobe, 1993). Later, MAP65 proteins from carrot (*Daucus carota*) and Arabidopsis have been identified that also form filamentous cross-bridges of 25 to 30 nm in between adjacent microtubules, corresponding to the distance in between microtubules reported for bundles in the cortex (Hardham and Gunning, 1978; Chan et al., 1999; Smertenko et al., 2004).

AtMAP65-1-GFP and AtMAP65-5-GFP had a tendency to associate with coaligned microtubules in elongated BY-2 cells and less with oblique microtubules in other cells. Thus, microtubule-binding activity of AtMAP65-1 and AtMAP65-5 depended on the overall organization of the microtubules. In fully expanded BY-2 cells, nearly all microtubules are transverse, and the colocalization of AtMAP65-1-GPF and AtMAP65-5-GFP with the microtubule marker TUA-2-RFP was virtually complete. This suggests that AtMAP65-1 and AtMAP65-5 are either implicated in the process of alignment of cortical microtubules, or their increased binding to microtubules coincides with the emergence of that particular organization. If and how AtMAP65 protein contributes to microtubule organization in the cortex is not really clear, but some hints follow from AtMAP65-1-GFP and AtMAP65-5-GFP time-lapse observations. The AtMAP65-1-GFP and AtMAP65-5-GFP transgenic cells generated fewer newly appearing fluorescent tracks in a fixed frame over the same time period than GFP-MBD and EtB1-GFP lines. We could think of two possible explanations for this observation. AtMAP65-1-GFP and AtMAP65-5-GFP may not bind to single microtubules until a second microtubule polymerizes along the same path or another individual microtubule joins in (see e.g. Fig. 5E). In this situation, single microtubule tracks would simply not be observed. Or MAP65 may promote the initiation of microtubules along existing microtubules, resulting in a reduction of microtubule tracks that appear independent of other microtubules. Cortical microtubules initiate at the cell cortex at positions in close association with existing microtubules and in regions where no other microtubules are detected (Shaw et al., 2003; our observations). AtMAP65-1-GFP and AtMAP65-5-GFP microtubules indeed appeared thicker than those ordinarily labeled with TUA2-RFP. Unfortunately, the microtubule dynamics within the cortical bundles were too complex and bleaching effects too strong in cells expressing GFP-tagged MAP65 together with the TUA2-RFP marker to allow accurate recording of the frequency of initiation events along existing microtubules. Nonetheless, the abundance of polymerization and depolymerization events suggests that initiation in association with microtubules was by the least not suppressed in cells producing AtMAP65-1-GFP.

Coalignment of microtubules can also be promoted by sustaining coincidental alignments once they are established. Two lines of evidence support a role for AtMAP65-1 and AtMAP65-5 in the stabilization of microtubules. Firstly, microtubules labeled with AtMAP65-1-GFP and AtMAP65-5-GFP displayed increased resistance against microtubule-destabilizing drugs. An intermediate resistance was observed in cells treated with oryzalin and amiprophos-methyl, two potent microtubule-destabilizing components of a similar class (Morejohn, 1991). Stronger protection was obtained against propyzamide that has a tubulin-binding site distinct from that of amiprophos-methyl (Young and Lewandowski, 2000). At low concentrations, propyzamide affects microtubule organization and leads to left-handed helical twisting of the cortical array in Arabidopsis epidermal cells (Furutani et al., 2000). Together these data suggest that propyzamide specifically attacks a position in microtubules that interacts with AtMAP65-1 protein. Secondly, microtubules labeled with AtMAP65-1-GFP and AtMAP65-5-GFP shrunk with half the rate of what was measured for GFP-MBD-labeled microtubules. A reduction in shrinkage rate of AtMAP65-labeled microtubules increases the life span of the microtubules. The rescue parameter was significantly reduced in cells producing AtMAP65-1-GFP and AtMAP65-5-GFP. This could lead to a reduction in the number of unstable microtubules with a net positive effect on the number of stable microtubules. The bundling activity of MAP65-1 by itself may not underlie the mechanism by which depolymerization is reduced, as normal rates were recorded for in vitro reconstituted microtubules decorated with AtMAP65-1 (Smertenko et al., 2004). Additional proteins dependent on AtMAP65-1 may be responsible for slowing down depolymerization.

The polymerization speed was not altered to that of control or the in vitro analyses recently reported (Smertenko et al., 2004). Proteins bound to the microtubule plus end, like, for example, the end-binding protein EB1, regulate the growth rate of microtubules (Tirnauer et al., 1999; Ligon et al., 2003). Arabidopsis has three EB1-like proteins, AtEB1a, AtEB1b, and AtEB1c, which were recently subcellularly localized (Chan et al., 2003; Mathur et al., 2003; Van Damme et al., 2004). AtEB1a-GFP and AtEB1b-GFP concentrate at the plus end, but also label the minus end and the endomembrane system, respectively. A further distinction between these EB1 homologous follows from the calculated polymerization rates, showing that AtEB1a-GFP-labeled microtubules grow significantly faster, consistent with the stimulatory effect of the yeast BIM1 and mammalian EB1 proteins on microtubule polymerization (Tirnauer et al., 1999; Ligon et al., 2003).

The microtubule-bundling activity assigned to recombinant AtMAP65-1 protein of in vitro turbidity polymerization assays is in line with our findings, showing a preferred incorporation of the AtMAP65-1-GFP protein into adjacent microtubules (Smertenko et al., 2004). The polarity of microtubules in the cortical array is not uniform (Tian et al., 2004). However, it was not clear whether bundles would consist of a mixture of parallel and antiparallel microtubules (Wicker-Planquart et al., 2004). Microtubules were observed to polymerize within existing bundles in two directions, which means that microtubules in a bundle are arranged in a parallel and in an antiparallel fashion. Whether AtMAP65-1 and AtMAP65-5 proteins selectively bundle either of these arrangements is not known, but the concentration of AtMAP65-1-GFP along microtubules was in accordance with the density of RFP-MBD and appears to depend on the presence of at least two coaligned microtubules. Vertebrate PRC1 and yeast Ase1 share sequence similarity with MAP65 proteins and show microtubule-bundling activity (Mollinari et al., 2002; Schuyler et al., 2003). They both specifically localize to the midzone where spindle microtubules overlap, suggesting that the bundling activity is directed to antiparallel-arranged microtubules. Immunocytological detection in a dividing cell localizes AtMAP65-3 to a narrow band at the midline of the phragmoplast, where microtubule plus ends congregate (Müller et al., 2004). AtMAP65-1 and AtMAP65-5 also associate with the phragmoplast, albeit more dispersed than AtMAP65-3 (Smertenko et al., 2004; Van Damme et al., 2004). As the phragmoplast may contain stretches of antiparallel-arranged microtubules, there is no evidence for bundling of parallel-aligned microtubules.

AtMAP65-1-GFP concentrated at spots that appeared to coincide with the end of a microtubule or a microtubule bundle. The overexpression of GFP-fusion proteins can lead to artificial localization patterns or result in, for instance, the formation of aggregates. However, the occurrence of fluorescent dots did not correlate with the expression level, as they were also seen in cell lines showing low fluorescence. The frequency at which highly fluorescent dots occurred depended on microtubule arrangement and increased when cells were treated with tubulin drugs. Under these conditions, cells presumably have shorter microtubules and therefore contain more microtubule termini. This would mean that in fully differentiated cells with very few dots, microtubules are much longer than was previously reported (Hardham and Gunning, 1978). Some dots were not visibly associated with microtubules. Perhaps in these cases, the microtubules were ultrashort yet numerous enough to bind AtMAP65-1-GFP, or the protein was trapped in aggregates. Whether AtMAP65-1 truly binds to fixed microtubule ends needs to be established by other techniques like, for example, electron microscopy.

According to microarray datasets, AtMAP65-1 and AtMAP65-5 are expressed throughout the cell cycle, and RNA levels slightly increased or decreased respectively upon release from the aphidicolin block. Yet, the localization data show that both proteins are selectively targeted to distinct consecutive mitotic configurations (Smertenko et al., 2004; Van Damme

et al., 2004). Hence, microtubule binding is differentially controlled throughout the cell cycle, possibly through posttranslational modification. In contrast with other AtMAP65 genes, AtMAP65-4 transcription was strongly up-regulated at the beginning of mitosis. The mitosis-specific expression of AtMAP65-4 correlates well with a strict targeting of AtMAP65-4-GFP to the perinuclear region in prophase cells and the spindle. The presence of a consensus D box in AtMAP65-4 points to a possible 26S proteasome-dependent degradation at the onset of anaphase. Since AtMAP65-4-GFP did not label the cortical array or the phragmoplast, its subcellular localization pattern opposes that of AtMAP65-1 and AtMAP65-5. For future studies it will be critical to identify the regulatory mechanisms by which MAP65 microtubule-binding activity is modulated.

MATERIALS AND METHODS

Fluorescent Protein Fusion Constructs and Transformation

AtMAP65-1, AtMAP65-4, AtMAP65-5, AtEB1a, and AtEB1b were cloned into the GATEWAY entry vector pDONR207 (Invitrogen, Carlsbad, CA; Van Damme et al., 2004). The open reading frames of TUA2, TUA6, and the MDB of MAP4 were amplified by PCR and cloned into pDONR221. For amplification of TUA2 and TUA6, the same set of primers was used. Primers were compatible with the GATEWAY vector and no adaptor sequences were included: TUA2/6-FWD, ATGAGAGAGTGCATTTCGATCCACA; TUA2/6-REV, TTAGTATTCCTCTCCTTCATCATCC; MBD-FWD, TCCCGGCA AGAAGAAGCAAAGG; MBD-REV, TTAACCTCCTGCAGGAAAGTGG-CCA. 35S promoter-driven GFP-fusion constructs were generated in the destination vector pK7FWG2 for C-terminal fusions and pH7WGR2 for N-terminal fusions via LR reactions (GATEWAY; Karimi et al., 2002, 2005). RFP-fusion constructs were made similarly, except that in the destination vector GFP was substituted with RFP. Stable BY-2 transformation was carried out as described (Geelen and Inzé, 2001). Tobacco leaf epidermal cells were transfected as described (Geelen et al., 2002).

Confocal Microscopy

Fluorescence microscopy was done with a confocal microscope 100M with software package LSM 510 version 3.2 (Zeiss, Jena, Germany), equipped with a 63× water corrected objective (numerical aperture of 1.2) to scan the cell cortex and the middle of dividing BY-2 cells. Dual GFP and RFP fluorescence was imaged in a multichannel setting with 488 nm and 543 nm light for GFP and RFP excitation, respectively. Emission fluorescence was captured in the frame-scanning mode alternating GFP fluorescence via a 500- to 550-nm bandpass emission filter and RFP via a 560-nm cutoff filter. Images were recorded at 3× to 5× digital zoom.

Immunostaining

Four days after subculture, TUA6-GFP and AtMAP65-5-GFP BY-2 cells were fixed and processed for immunolabeling with anti-α-tubulin monoclonal antibodies (1:3,000; Molecular Probes, Eugene, OR) according to the procedure described in Ritzenthaler et al. (2002).

Drug Treatments

For live cell recordings, samples were applied to a chambered cover glass (Lab-Tek, Naperville, IL) and immobilized in a thin layer of 200 μL of BY-2 medium containing vitamins and 1.6% of low-melting-point agar (Invitrogen). Selected cells were imaged before the addition of oryzalin (10 μM final concentration), amiprophos-methyl (10 μM final concentration; Duchefa, Haarlem, The Netherlands), or propyzamide (6 μM final concentration; Chem Service, West Chester, PA). Drugs were added in a volume of 1,000 μL of BY-2 medium with added vitamins and the drug at a concentration adjusted to a final volume of 1,200 μL. Stock solutions of APM (10 mM) and propyzamide (600 μM) were dissolved in dimethylsulfoxide. As control, 1,000× and 100× dimethylsulfoxide dilutions in BY-2 medium were used. Microtubule behavior was monitored in consecutive image stacks taken 30 min and 2 h after drug application.

Microtubule Track Measurements

The cell cortex was monitored over the course of 10 min and imaged every 10 s (60 images). The number of fluorescent tracks in these time-lapse recordings (AtMAP65-1, $n = 16$; AtMAP65-5, $n = 20$; AtEB1A, $n = 19$ and GFP-MBD, $n = 26$) that crossed a straight 20-μm line placed perpendicular to the main axis of the transversely oriented microtubules was counted. Fluorescence intensity of microtubule tracks was measured on single optical sections or flattened Z-stack images averaged for fluorescence intensity (Fig. 4), using the ImageJ software program (http://rsb.info.nih.gov/ij/). Data points were collected from individual microtubule tracks and resliced against time as kymographs. Fluorescence intensity variations in microtubule bundles were plotted as the respective gray value of the EGFP/RFP fluorescence against the position within a track.

Quantification of Microtubule Dynamic Instability Parameters

Cells preincubated for 12 h in chambered cover-glass wells (Lab-Tek) were recorded in solidified BY-2 medium containing 1.6% low-melting-point agar (Invitrogen) at room temperature. Images were taken every 10 s during the course of 10 min. Growth and shrinkage velocities were calculated by dividing the distance covered by the time spent for growth or shortening. Polymerization rates were averaged from at least three individual measurements per cell. A minimum of 49 and a maximum of 120 events were analyzed from 13 up to 20 different cells. ANOVA and Scheffe statistical tests indicated that the average polymerization rates calculated for microtubules labeled with AtMAP65, AtEB1b, and GFP-MBD fell into a single category and that they were significantly distinct from that of the AtEB1a-labeled microtubules. Depolymerization rates were calculated from a minimum of 36 and maximum of 58 individual events. ANOVA and Scheffe tests indicated that the average depolymerization rates of microtubules labeled with AtMAP65-1-GFP and AtMAP65-5-GFP were statistically distinct from those labeled with GFP-MBD. Frequency of catastrophy and rescue (events s^{-1}) were calculated as the inverse of the mean time spent in depolymerization and in polymerization, respectively (Cassimeris et al., 1988).

ACKNOWLEDGMENT

We thank Roger Tsien for the RFP clone pRSETb.

Received August 22, 2004; returned for revision October 11, 2004; accepted October 11, 2004.

LITERATURE CITED

Anthony RG, Hussey PJ (1999) Dinitroaniline herbicide resistance and the microtubule cytoskeleton. Trends Plant Sci **4:** 112–116

Campbell RE, Tour O, Palmer AE, Steinbach PA, Baird GS, Zacharias DA, Tsien RY (2002) A monomeric red fluorescent protein. Proc Natl Acad Sci USA **99:** 7877–7882

Cassimeris L, Pryer NK, Salmon ED (1988) Real-time observations of microtubule dynamic instability in living cells. J Cell Biol **107:** 2223–2231

Chan J, Calder GM, Doonan JH, Lloyd CW (2003) EB1 reveals mobile microtubule nucleation sites in *Arabidopsis*. Nat Cell Biol **5:** 967–971; erratum **Chan J, Calder GM, Doonan JH, Lloyd CW** (2004) Nat Cell Biol **6:** 77

Chan J, Jensen CG, Jensen LCW, Bush M, Lloyd CW (1999) The 65-kDa carrot microtubule-associated protein forms regularly arranged fila-

mentous cross-bridges between microtubules. Proc Natl Acad Sci USA **96:** 14931–14936

Chang-Jie J, Sonobe S (1993) Identification and preliminary characterization of a 65 kDa higher-plant microtubule-associated protein. J Cell Sci **105:** 891–901

Criqui MC, Parmentier Y, Derevier A, Shen W-H, Dong A, Genschik P (2000) Cell cycle-dependent proteolysis and ectopic overexpression of cyclin B1 in tobacco BY2 cells. Plant J **24:** 763–773

Cyr RJ, Palevitz BA (1995) Organization of cortical microtubules in plant cells. Curr Opin Cell Biol **7:** 65–71

Dhonukshe P, Gadella TWJ Jr (2003) Alteration of microtubule dynamic instability during preprophase band formation revealed by yellow fluorescent protein-CLIP170 microtubule plus-end labelling. Plant Cell **15:** 597–611

Furutani I, Watanabe Y, Prieto R, Masukawa M, Suzuki K, Naoi K, Thitamadee S, Shikanai T, Hashimoto T (2000) The *SPIRAL* genes are required for directional control of cell elongation in *Arabidopsis thaliana*. Development **127:** 4443–4453

Geelen D, Leyman B, Batoko H, Di Sansabastiano G-P, Moore I, Blatt MR (2002) The abscisic acid-related SNARE homolog NtSyr1 contributes to secretion and growth: evidence from competition with its cytosolic domain. Plant Cell **14:** 387–406

Geelen DNV, Inzé DG (2001) A bright future for the Bright Yellow-2 cell culture. Plant Physiol **127:** 1375–1379

Genschik P, Criqui MC, Parmentier Y, Derevier A, Fleck J (1998) Cell cycle-dependent proteolysis in plants: identification of the destruction box pathway and metaphase arrest produced by the protease inhibitor MG132. Plant Cell **10:** 2063–2075

Goddard RH, Wick SM, Silflow CD, Snustad DP (1994) Microtubule components of the plant cell cytoskeleton. Plant Physiol **104:** 1–6

Hardham AR, Gunning BES (1978) Structure of cortical microtubule arrays in plant cells. J Cell Biol **77:** 14–34

Hush JM, Wadsworth P, Callaham DA, Hepler PK (1994) Quantification of microtubule dynamics in living plant cells using fluorescence redistribution after photobleaching. J Cell Sci **107:** 775–784

Hussey PJ, Hawkins TJ, Igarashi H, Kaloriti D, Smertenko A (2002) The plant cytoskeleton: recent advances in the study of the plant microtubule-associated proteins MAP-65, MAP-190 and the *Xenopus* MAP215-like protein, MOR1. Plant Mol Biol **50:** 915–924

Ito M, Iwase M, Kodama H, Lavisse P, Komamine A, Nishihama R, Machida Y, Watanabe A (1998) A novel *cis*-acting element in promoters of plant B-type cyclin genes activates M phase-specific transcription. Plant Cell **10:** 331–341

Karimi M, Inzé D, Depicker A (2002) GATEWAY vectors for *Agrobacterium*-mediated plant transformation. Trends Plant Sci **7:** 193–195

Karimi M, De Meyer B, Hilson P (2005) Modular cloning in plants. Trends Plant Sci **10:** (in press)

Ligon LA, Shelly SS, Tokito M, Holzbaur ELF (2003) The microtubule plus-end proteins EB1 and dynactin have differential effects on microtubule polymerization. Mol Biol Cell **14:** 1405–1417

Lloyd C, Chan J (2004) Microtubules and the shape of plants to come. Nat Rev Mol Cell Biol **5:** 967–971

Mathur J, Mathur N, Kernebeck B, Srinivas BP, Hülskamp M (2003) A novel localization pattern for an EB1-like protein links microtubule dynamics to endomembrane organization. Curr Biol **13:** 1991–1997

Menges M, Hennig L, Gruissem W, Murray JAH (2003) Genome-wide gene expression in an *Arabidopsis* cell suspension. Plant Mol Biol **53:** 423–442

Mollinari C, Kleman J-P, Jiang W, Schoehn G, Hunter T, Margolis RL (2002) PRC1 is a microtubule binding and bundling protein essential to maintain the mitotic spindle midzone. J Cell Biol **157:** 1175–1186

Moore RC, Zhang M, Cassimeris L, Cyr RJ (1997) In vitro assembled plant microtubules exhibit a high state of dynamic instability. Cell Motil Cytoskeleton **38:** 278–286

Morejohn LC (1991) The molecular pharmacology of plant tubulin and microtubules. *In* CW Lloyd, ed, The Cytoskeletal Basis of Plant Growth and Form. Academic Press, San Diego, pp 29–44

Müller S, Smertenko A, Wagner V, Heinrich M, Hussey PJ, Hauser M-T (2004) The plant microtubule-associated protein AtMAP65-3/PLE is essential for cytokinetic phragmoplast function. Curr Biol **14:** 412–417

Ritzenthaler C, Nebenführ A, Movafeghi A, Stussi-Garaud C, Behnia L, Pimpl P, Staehelin LA, Robinson DG (2002) Reevaluation of the effects of brefeldin A on plant cells using tobacco Bright Yellow 2 cells expressing Golgi-targeted green fluorescent protein and COPI antisera. Plant Cell **14:** 237–261

Schuyler SC, Liu JY, Pellman D (2003) The molecular function of Ase1p: evidence for a MAP-dependent midzone-specific spindle matrix. J Cell Biol **160:** 517–528

Shaul O, Mironov V, Burssens S, Van Montagu M, Inzé D (1996) Two *Arabidopsis* cyclin promoters mediate distinctive transcriptional oscillation in synchronized tobacco BY-2 cells. Proc Natl Acad Sci USA **93:** 4868–4872

Shaw SL, Kamyar R, Ehrhardt DW (2003) Sustained microtubule treadmilling in *Arabidopsis* cortical arrays. Science **300:** 1715–1718

Smertenko A, Saleh N, Igarashi H, Mori H, Hauser-Hahn I, Jiang C-J, Sonobe S, Lloyd CW, Hussey PJ (2000) A new class of microtubule-associated proteins in plants. Nat Cell Biol **2:** 750–753

Smertenko AP, Chang H-Y, Wagner V, Kaloriti D, Fenyk S, Sonobe S, Lloyd C, Hauser M-T, Hussey PJ (2004) The Arabidopsis microtubule-associated protein AtMAP65-1: molecular analysis of its microtubule bundling activity. Plant Cell **16:** 2035–2047

Tian G-W, Smith D, Glück S, Baskin TI (2004) Higher plant cortical microtubule array analyzed in vitro in the presence of the cell wall. Cell Motil Cytoskeleton **57:** 26–36

Tirnauer JS, O'Toole E, Berrueta L, Bierer BE, Pellman D (1999) Yeast Bim1p promotes the G1-specific dynamics of microtubules. J Cell Biol **145:** 993–1007

Van Damme D, Bouget F-Y, Inzé D, Geelen D (2004) Identification of new phragmoplast proteins through GFP-fluorescence profiling of plant cell division related proteins. Plant J **40:** 386–398

Vantard M, Schellenbaum P, Peter C, Lambert AM (1993) Higher plant microtubule-associated proteins: *in vitro* functional assays. Biochimie **75:** 725–730

Wasteneys GO (2002) Microtubule organization in the green kingdom: chaos or self-order? J Cell Sci **115:** 1345–1354

Wicker-Planquart C, Stoppin-Mellet V, Blanchoin L, Vantard M (2004) Interactions of tobacco microtubule-associated protein MAP65-1b with microtubules. Plant J **39:** 126–134

Yasuhara H, Muraoka M, Shogaki H, Mori H, Sonobe S (2002) TMBP200, a microtubule bundling polypeptide isolated from telophase tobacco BY-2 cells is a MOR1 homologue. Plant Cell Physiol **43:** 595–603

Young DH, Lewandowski VT (2000) Covalent binding of the benzamide RH-4032 to tubulin in suspension-cultured tobacco cells and its application in a cell-based competitive-binding assay. Plant Physiol **124:** 115–124